

# Optimization of Heat Transfer in an Enclosure with a Trombe Wall and Solar Chimney

A.R. Shateri<sup>1</sup>, I. Pishkar<sup>2\*</sup> and Sh. Mohammad Beigi<sup>1</sup>

1. Mechanical Engineering Department, Engineering Faculty of Shahrekord University, Shahrekord, Iran.

2. Department of Mechanics, Payame Noor University, Tehran, Iran.

Receive Date 05 November 2021; Revised 14 November 2021; Accepted Date 11 December 2022

\*Corresponding author: E.pishkar@pnu.ac.ir (I. Pishkar)

## Abstract

Trombe walls and solar chimneys have been widely used in the construction industry for many years in order to heat the buildings. In this work, the heat conductance of a Trombe wall is simulated and studied. The equations related to energy and momentum are solved numerically using the technique of control volume. The equations are solved simultaneously using the Simple algorithm. At first, a base case is defined and simulated. A sensitivity analysis study is then performed in order to investigate the parameters affecting the performance of the wall. Based on the results obtained, an optimized geometry is suggested, which maximizes the performance of the Trombe wall. In addition, the effect of the presence of the fins on the surface of the absorber wall is studied. In order to obtain the best geometry, the fins are assumed to have different shapes but with a constant area. The results obtained show that the Trombe wall with rectangular fins demonstrate the best performance compared to the other fin geometries studied in this work. The presence of rectangular fins can increase the room temperature by 1.24% compared to the other fin geometries.

**Keywords:** Optimization, Trombe wall, Solar chimney, Numerical simulation, Fin.

## 1. Introduction

The construction industry is one of the sectors with the highest energy consumption in both the developing and developed countries [1-3]. More than one-third of the total energy is consumed in the houses and other buildings [4, 5]. Most of this energy is used for heating, cooling, and ventilation of the houses and buildings [6]. Hence, the design and application of the non-active methods of heating can significantly reduce energy consumption. Using solar power for heating can be categorized as one of these non-active methods, which are widely used all around the world [7-9]. There are two methods for heating a building using solar power: passive and active [10-12].

In the active design, a liquid transports the solar heat so it requires another source of energy in order to circulate the heated liquid inside the house [13]. In the passive design, the building absorbs the solar power directly; hence, the architecture of the building is a key factor in determining the total absorption of the energy [14]. In this method, the windows, walls, and floors are designed to absorb, accumulate, and

circulate the solar energy in the building during the winter times [15]. However, these elements also reflect the solar energy during summer to help maintain the building at a low temperature. In contrast with the active solar systems, the passive systems do not require any other electrical equipment to circulate the heated liquid inside the building [16]. Hence, the consumption of fossil fuels is minimized in these systems. The solar walls are based on the concept of a chimney effect in an air gap, and are categorized as passive designs to use solar power in order to heat the buildings. The Trombe wall was named after the French researcher Felix Trombe, who designed and used these walls in 1966 [17, 18].

This system is similar to a heavy wall; however, several vents are located at the top and the bottom of the Trombe wall. These vents allow the circulation of the hot air adjacent to the wall and the cool air inside the building by natural convection (Figure 1 [19]). The Trombe wall usually faces south in the northern hemisphere in order to maximize the absorption of solar energy. The Trombe wall consists of an absorbing wall

and a glass surface. The absorber is located within a short distance from the glass surface, and is filled with high-density materials such as rocks, clay, bricks or paraffin wax. The solar energy is absorbed by the absorber, which has a high thermal capacity and a high radiation absorption coefficient. In this geometry, the air flows from the vents located at the top and the bottom of the Trombe wall. The heat absorbed by the wall heats the ambient air flowing through the gaps between the wall and the glass surface. The heated air is circulated in the system, and enters the room due to the chimney effect and natural convection [20, 21].

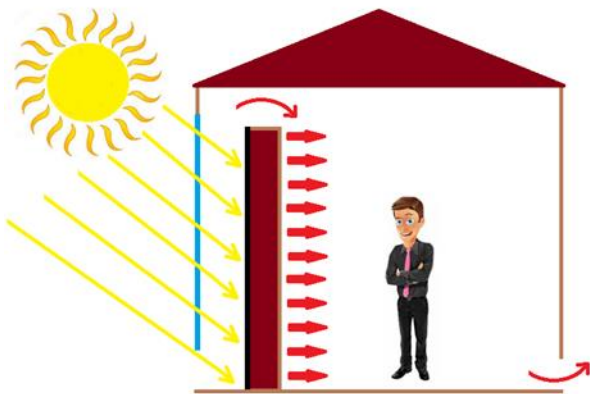


Figure 1. A simple diagram of a Trombe wall [19].

There have been many studies on the use of a non-active method like solar walls and solar ceilings. Chan *et al.* (2010) have introduced and discussed different methods of non-active solar systems such as solar chimneys, solar walls, solar windows, and solar ceilings [22]. Yedder *et al.* (1990) have studied the laminar natural convection in a composite solar wall. They used the simpler method, and showed that the ratio of width to height in solar walls does not affect the system performance [23]. Later, they used the finite volume method in order to solve the equations of laminar flow and natural convection in the solar wall [24]. Gan (2006) has used the Fluent software for simulation and examination of the effect of the buoyancy force on natural convection in a rectangular container [25], while Mezrhab and Rabhi (2008) have included the radiation equations as well as natural convection in their simulations. They concluded that radiative exchanges decreased the temperature gradients and result in an increase in the average Nusselt number and the airflow via the openings. In addition, the increase in the dimensionless width of the opening leads to an increase in the heat transfer within the cavity [26].

Li *et al.* (2007) have revealed that the most important parameter in heat adsorption is the width of the air gap between the Trombe wall and the glass surface [27]. Kim and Seo (2012) have used the finite volume method in their fluid dynamic simulations, investigating the effect of changing the vents' position at the top and the bottom of the solar wall [28]. Tan and Wong have used the Fluent software in order to simulate the solar chimneys in regions with a high temperature and moisture, investigating the temperature effect on the system efficiency [20].

Some researchers have suggested an analytical solution for the heat transfer equation of the natural convection in an unsteady state laminar flow [29, 30]. Ong has used a network of thermal resistors for the simulation of a 1D solar chimney and Trombe wall [31]. Haghghi and Maerefat (2014) have investigated the solar ventilation and heating of a building in the sunny days of winter. They simulated the solar chimney performance, and studied the effect of outside temperature on its performance. They concluded that by increasing the air gap between the absorber and the glass surface, the room temperature decreased over a longer time [32].

Although many researchers have simulated and studied these solar systems in the literature, the geometry of the Trombe wall has not been studied extensively. In this work, we tried to simulate and study the performance of the Trombe walls with different geometries. All the three mechanisms of the heat transfer (radiation, convection, and conduction) were simulated in order to mimic the real physics of the system. Moreover, all the effective parameters in the geometry of the Trombe wall were studied in order to find the conditions with an optimal performance, and to obtain the highest temperature in the room. In this work, the initial problem is stated, and the suggested geometries are described. The mathematical model used in the simulation and the boundary conditions is then discussed. The validation of the results obtained is then explained, and it is shown that the results obtained are grid-independent. Finally, the effect of each geometry type on the average room temperature is explained. Some of the other parameters studied in this work are the number of the fins, increase in the radiation power, increase in the width of the air gap, and locations of the vents.

## 2. Mathematical description

In this research work, an attempt is made to design the solar wall and its materials for an optimal use of the solar energy in winter in order

to heat the buildings [33]. The assumed geometry of the solar chimney is shown in figure 2. The room is assumed to be 2D and its area is 4\*4 square meters. The southern wall of the solar chimney faces the sunlight. The basic assumption is that the wall is made of glass in order to increase the heat flux and the sunlight. The northern wall is assumed to be made of clay to increase the absorption, and provide a steeper heat gradient through the wall. The properties of the walls are shown in table 1. In addition, the room has two inlet and outlet vents for the air flow, and their sizes are 0.2 m and 0.5 m, respectively. The thickness of the wall is constant, and equal to 0.2 m. However, the dimensions of the air gap and the distance between the absorber and the glass surface are assumed as variables. Later, several fins with rectangular, triangular, and circular shapes were mounted on the absorber surface, and the results obtained were studied

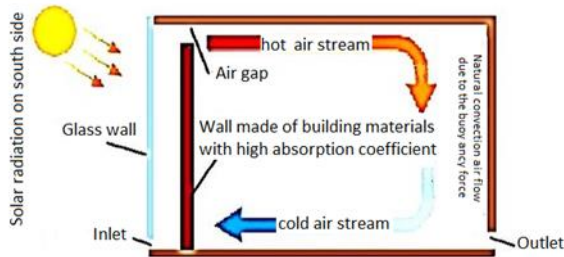


Figure 2. A schematic representation of solar chimney used in the simulations.

Table 1. Characteristics of materials utilized in simulation of solar chimney [34].

Material	Density (kg/m <sup>3</sup> )	Thermal conductivity (w/m.k)	Specific heat transfer (j/kg.k)
Air	1.225	0.0242	1006.43
Brick	1700	0.69	840
Glass	2203	1.05	840

### 3. Formulations used in simulations

It is assumed that the phenomena of fluid and heat transfer in the solar chimney and the room are governed by the 2D Navier-Stokes equations. The same assumption applies to the energy equation. The fluid is assumed to be an incompressible fluid that satisfies the Boussinesq approximation. This means that except for the buoyancy term of the motion equation, the variation of density with temperature is insignificant. All the other thermodynamic and transport properties of the fluid are assumed constant, as well as the compression work, viscous dissipation, and radiative transport, which are negligible and equal to zero. The governing equations are [35]:

Conservation of mass:

$$\frac{\partial(\rho\bar{u})}{\partial x} + \frac{\partial(\rho\bar{v})}{\partial y} = 0 \quad (1)$$

Conservation of x-momentum [36, 37]:

$$\begin{aligned} \frac{\partial(\rho\bar{u}\bar{u})}{\partial x} + \frac{\partial(\rho\bar{u}\bar{v})}{\partial y} = & -\frac{\partial P}{\partial x} + \frac{\partial}{\partial x}((\mu + \mu_t)\frac{\partial\bar{u}}{\partial x}) \\ & + \frac{\partial}{\partial y}((\mu + \mu_t)\frac{\partial\bar{u}}{\partial y}) - \frac{2}{3}\rho\frac{\partial k}{\partial x} \end{aligned} \quad (2)$$

Conservation of y-momentum [36, 37]:

$$\begin{aligned} \frac{\partial(\rho\bar{u}\bar{v})}{\partial x} + \frac{\partial(\rho\bar{v}\bar{v})}{\partial y} = & -\frac{\partial P}{\partial y} + \frac{\partial}{\partial x}((\mu + \mu_t)\frac{\partial\bar{v}}{\partial x}) \\ & + \frac{\partial}{\partial y}((\mu + \mu_t)\frac{\partial\bar{v}}{\partial y}) - \frac{2}{3}\rho\frac{\partial k}{\partial y} + (\rho - \rho_0)g \end{aligned} \quad (3)$$

Conservation of energy:

$$\begin{aligned} \frac{\partial(\rho\bar{u}T_f)}{\partial x} + \frac{\partial(\rho\bar{v}T_f)}{\partial y} = & \frac{\partial}{\partial x}\left(\left(\frac{\lambda}{C_p} + \frac{\mu_t}{pr_t}\right)\frac{\partial T_f}{\partial x}\right) \\ & + \frac{\partial}{\partial y}\left(\left(\frac{\lambda}{C_p} + \frac{\mu_t}{pr_t}\right)\frac{\partial T_f}{\partial y}\right) \end{aligned} \quad (4)$$

in which,  $\mu_t$  is the turbulent dynamic viscosity, and is calculated using the equation below [38, 39]:

$$\mu_t = c_\mu f_\mu \frac{\rho k^2}{e} \quad (5)$$

$f_\mu$  is the wall damping function:

$$\begin{aligned} f_\mu = & 1 - \exp(-a_1 Re_y - a_2 Re_y^3 - a_3 Re_y^5)^{0.5} \\ a_1 = & 1.5 \times 10^{-4}, a_2 = 5 \times 10^{-7}, \\ a_3 = & 1.0 \times 10^{-10}, Re_y = k^{0.5} y^+ / \nu \end{aligned} \quad (6)$$

$Re_y$  is the turbulent Reynolds number near the absorber wall. It changes very slowly along the lines parallel to the wall; however, it does not disappear at separation, and remains well-defined even in the regions of flow reversal. Hence, the models with a low Reynolds number require very fine grids at the walls. Usually the first node is located at distances less than 1 ( $y^+ < 1$ ) from the wall. In order to decrease the turbulence equation stiffness, and to reduce the number of grid points, the coarser grids are assumed at distances between 10 and 100 ( $10 < y^+ < 100$ ) [40].

Turbulent kinetic energy [35]:

$$\begin{aligned} \frac{\partial(\rho\bar{u}k)}{\partial x} + \frac{\partial(\rho\bar{v}k)}{\partial y} = & \frac{\partial}{\partial x}((\mu + \mu_t / \sigma_k)\frac{\partial k}{\partial x}) + \\ & \frac{\partial}{\partial y}((\mu + \mu_t / \sigma_k)\frac{\partial k}{\partial y}) + P_k + G_b - \rho\epsilon - 2\nu\frac{\partial k^{0.5}}{\partial y} \end{aligned} \quad (7)$$

Turbulence dissipation [40]:

$$\frac{\partial(\rho\bar{u}e)}{\partial x} + \frac{\partial(\rho\bar{v}e)}{\partial y} = \frac{\partial}{\partial x} ((\mu + \mu_t / \sigma_e) \frac{\partial e}{\partial x}) + \frac{\partial}{\partial y} ((\mu + \mu_t / \sigma_e) \frac{\partial e}{\partial y}) + c_{1d} f_1 (P_k + c_{3e} G_b) - c_{2d} f_2 \rho e \frac{e^2}{k} + 2\mu\mu_t (\frac{\partial^2 u}{\partial y^2})^2 \quad (8)$$

$P_k$  and  $G_b$ , respectively, indicate the shearing production and the generation/destruction of the buoyancy turbulent kinetic energy [40]:

$$P_k = \mu_t (\frac{\partial u_i}{\partial x_j} + \frac{\partial u_j}{\partial x_i}) \frac{\partial u_i}{\partial x_j} - \frac{2}{3} \rho k \delta_{ij} \frac{\partial u_i}{\partial x_j} \quad (9)$$

$$G_b = \rho g_i \frac{\mu_t}{\rho r_i} \frac{\partial T_f}{\partial x_i} \quad (10)$$

In order to calculate the turbulent flow, the wall functions can be solved for calculation of the velocities and temperature as well as for  $k$  and  $e$ . In this work, the wall functions were regarded zero for  $k$  and  $e$ ; however, the other variables were calculated. For the standard  $k$ - $e$  models, the constants and other wall damping functions include the following values [41]:

$$C_{1e} = 1.44, C_{2e} = 1.92, C_{3e} = 1.0, C_\mu = 0.09, f_1 = 1.0, f_2 = 1.0, \sigma_k = 1.0, \sigma_e = 1.3 \quad (11)$$

An academic code was used to solve the governing equations.

### 3.1. Boundary conditions

The turbulence kinetic energy and the velocity were assumed to be zero at the walls [42, 43]. The outlet and inlet pressures were equal to zero in the system [44]. The boundary conditions of temperature were achieved according to thermal processes (Figure 3). The thermal inertia of the glass and the radiative heat absorption of the air were considered insignificant. Using the energy balance equation for glass surface, the glass temperature ( $T_g$ ) was calculated [45]:

$$S_g A_g + hr_{abs-g} A_{abs} (T_{abs} - T_g) = h_{g-fsc} A_g (T_g - T_{fsc}) + U_{g-a} A_g (T_g - T_a) \quad (12)$$

The heat loss coefficient from glass cover to ambient air ( $U_{g-a}$ ) was obtained using [45]:

$$U_{g-a} = h_{wind} + hr_{g-sky} \quad (13)$$

The convective heat transfer coefficient caused by wind was given by Duffie and Beckmann [46], as follows:

$$h_{wind} = 2.8 + 3u_{wind} \quad (14)$$

In order to calculate the solar radiation heat flux absorbed by the glass surface:

$$S_g = \alpha_g I \quad (15)$$

Considering the ambient temperature, the radiative heat transfer coefficient from the outer surface of the glass to the sky was calculated using [45]:

$$hr_{g-sky} = \frac{\sigma_r \epsilon_g (T_g + T_{sky})(T_g^2 + T_{sky}^2)(T_g - T_{sky})}{(T_g - T_a)} \quad (16)$$

$$T_{sky} = 0.0552 T_a^{1.5}$$

The radiative heat transfer coefficient between the absorber wall and the glass surface was:

$$hr_{abs-g} = \frac{\sigma_r (T_g^2 + T_{abs}^2)(T_g + T_{abs})}{(1/\epsilon_g + 1/\epsilon_{abs} - 1)} \quad (17)$$

The convective heat transfer coefficient between the glass surface and the air flowing inside the solar chimney ( $h_{g-fsc}$ ) was calculated using equation.

$$h_{g-fsc} (T_g - T_{fsc}) = -\lambda_{fsc} \frac{\partial T_{fsc}}{\partial x} \Big|_{x=0} \quad (18)$$

The coefficient of the convective heat transfer between the absorber wall and the airflow in the chimney is given by Eq. (19).  $T_{abs}$  was calculated from the energy balance equation for the absorber plate, Eq. (20):

$$h_{abs} (T_{fsc} - T_{abs}) = -\lambda_{fsc} \frac{\partial T_{fsc}}{\partial x} \Big|_{x=d_{sw}} \quad (19)$$

$$S_{abs} A_{abs} = h_{abs} A_{abs} (T_{abs} - T_{fsc}) + hr_{abs-g} A_{abs} (T_{abs} - T_g) + U_{abs-r} A_{abs} (T_{abs} - T_{fr}) \quad (20)$$

The overall heat transfer coefficient between the rear of the absorber wall to the air of the room ( $U_{abs-r}$ ) was calculated by:

$$U_{abs-r} = \frac{1}{(1/h_r + t_{ins} / \lambda_{ins})} \quad (21)$$

in which  $h_r$  is the coefficient of the convective heat transfer between the room air and insulation, calculated as:

$$U_{abs-r} A_{abs} (T_{abs} - T_{fr}) = -\lambda_{fr} \frac{\partial T}{\partial x} \Big|_{x=d_{sw} + t_{ins}} \quad (22)$$

Finally, the solar radiation heat flux absorbed by the absorber wall is:

$$S_{abs} = \alpha_{abs} I \quad (23)$$

In this work, the numerical simulations were performed in the steady state conditions because the changes in the ambient air temperature and the received radiation energy were very slow processes compared to the changes in the room temperature. Moreover, in this work, we aimed to examine the effect of geometry on the solar wall's performance and on the average room temperature. Hence, many parameters such as the radiation energy flux were required to be controlled in the simulations. The modified Simpler algorithm was used to solve the pressure and velocity equations simultaneously. The calculations were based on the typical weather conditions; hence, the average temperature of the outside was 10 °C in the winter, and the radiation power on the south facing glass was assumed to be 100, 200, and 500 (W/m<sup>2</sup>), and the direction was perpendicular to the glass surface [23]. The material radiation constants are shown in table 2.

**Table 2. Constant parameters in simulation of solar chimney [45].**

Material	Absorption coefficient ( $\alpha$ )	Diffusion coefficient ( $\epsilon$ )
Absorbent surface of brick	0.95	0.95
Glass	0.06	0.9

In this work, the conjugate heat transfer of the solid adsorber wall was considered to simulate the real physics of the system and avoid simplification. To the best of the authors' knowledge, these properties have not been paid attention to in many published papers in this field. Figure 3 illustrates the boundary conditions of the simulations. The boundary conditions are considered so that the static pressure and some of the variables of the flow equation can be determined. Figure 4 shows the algorithm used for the simulation in this work.

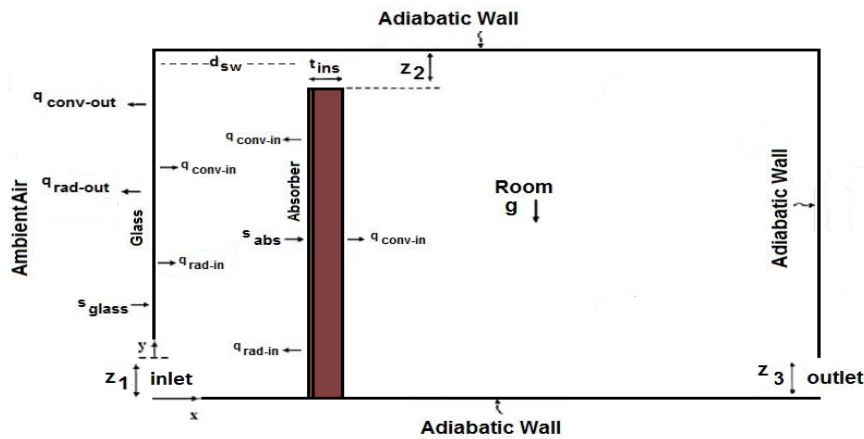


**Figure 3. Boundary conditions used in simulations.**

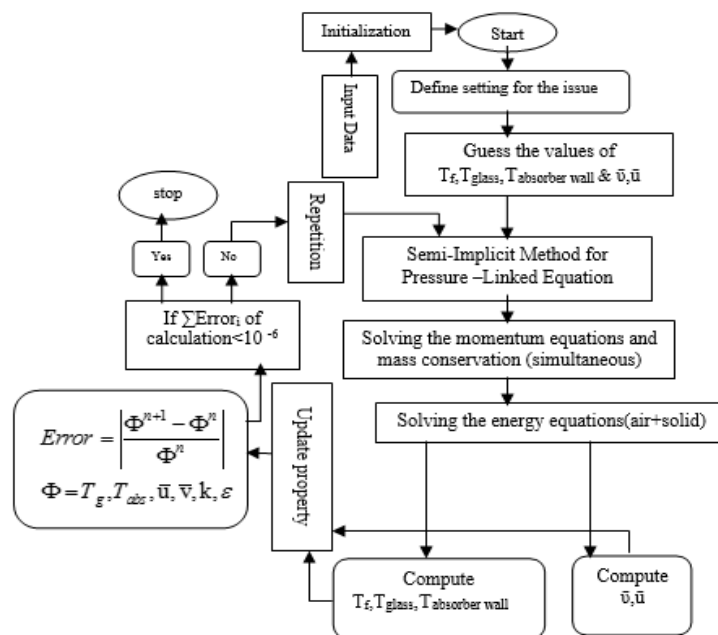


**Figure 4. A flow chart of algorithm used in simulations.**

#### 4. Validation of simulation results

In order to validate the results obtained, they were compared with the results reported by Haghghi *et al.* [32]. Their geometry was a 2D room with a Trombe wall that had two inlet and outlet vents. Figure 5 shows the comparison of the results of the average room temperature obtained in this research work with the data reported by Haghghi *et al.* The results obtained show a good match between the results achieved in this work and the results reported in the literature. Now the base case could be used to perform other simulations and add the fins to the surface of the absorber plate.

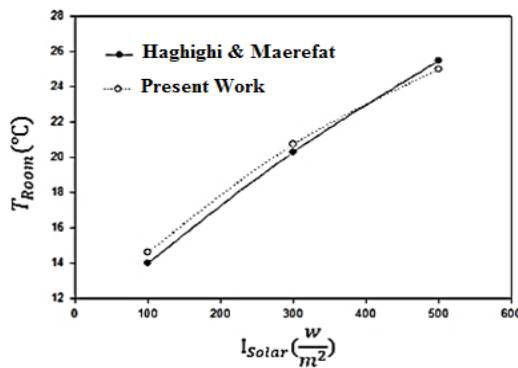


Figure 5. Comparison of results obtained in this work with results reported in the literature [32].

#### 5. Impact of grid size on results

In this part, a sensitivity analysis was performed in order to understand the effect of grid size on the results. The number of the grids defined on the surface was changed between 15\*15 and 90\*90, and the results obtained were compared. The objective was to find the largest grid size at which the results obtained were independent from the grid size. The velocity at the center-line of the room ( $x = 2m, 0 \leq y \leq 4m$ ) was used for comparison, and the results obtained were shown in figure 6. The graph shows that with mesh 60\*60 grids and more; the results are independent from the grid size.

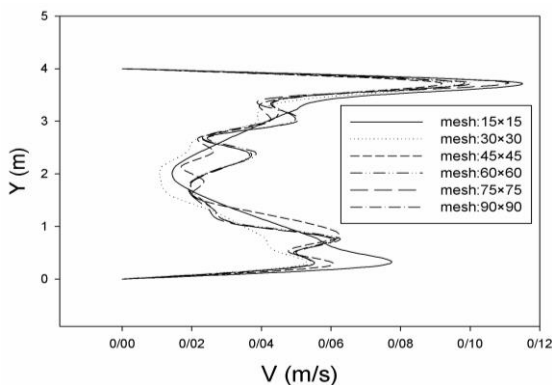


Figure 6. Impact of grid size on velocity calculated at center line of the room ( $x = 2 m, 0 \leq y \leq 4m$ ).

#### 6. Simulation results

In this section, the effect of several parameters on the temperature and stream/temperature contours were investigated. The parameters studied were the intensity of the radiation, height of the Trombe wall, shape of the fins, number of fins, location of the outlet vents, and e distance between the absorber wall and the glass surface.

##### 6.1. Effect of height of Trombe wall and shape of fins

Figures 7-9 show the isotherms and streamlines for the base case (absorber without fins) and the absorber with the triangular, semi-circular, and rectangular fins, respectively. These results obtained are shown at a radiation flux of 500 Watt per square meter ( $W/m^2$ ). The fins were used to increase the heat transfer when the heat conduction inside the material and the convection heat transfer from the fins occurred simultaneously. The heat conduction inside the fin directly affected the temperature gradient along the fin, and consequently, the rate of heat transfer. The dimensions of the fins were calculated so that the total area of the fins was equal in different geometries. The presence of the fins increased the area of the absorbing wall that was in direct sunlight. However, the area of the fins was assumed to be equal. The type of fin was determined according to the dimension and weight in order to increase the pressure drop or heat transfer. The streamlines showed the air circulation pattern in the room.

In the smaller air gaps, the pattern of air circulation was different for various geometries. As the air gap was expanded, the difference between the patterns of air circulation decreased and the streamline contours were more similar (Figures. 7-9). It is usually desired to have the fewest vortices in the room in order to provide the most comfortable conditions for the dwellers. The results obtained show that the use of the fins significantly reduces the vortices in the system.

As the air gap is increased, the room is more comfortable for the dwellers. The room becomes brighter since it receives more sunlight from the southern wall. The use of fins is more practical in larger air gaps since it results in an increase in the average room temperature without any changes to the room brightness. If the air gap size is reduced, the air flow through the vents located at the top and bottom of the solar chimney is not as effective as possible due to the frictional pressure drop across the small cross-section of the flow. On the other hand, at larger air gaps, the heat transfer is affected adversely due to the reduction in flow

velocity and the gradient of the temperature between the absorber wall and the glass surface, as shown in figures 7-9.

The comparison of the isotherm contours shows that the use of a rectangular fin shape results in the highest temperature in the room, while the lowest temperature is found in the base case with no fins present. Figure 10 shows the average room temperature calculated for different types of fins at different air gap distances. The temperature with the rectangular fin is the highest. The reason is that the disturbance and turbulence caused by rectangular fins are higher compared to the other types of fins. The manufacture and installation of rectangular fins is easier and cheaper than the other types of fins. Moreover, these fins are lighter at the same area compared to the other types. Hence, the rectangular fins are an appropriate solution to maximize the efficiency of the Trombe wall.

Comparison of the isotherms and the average room temperature (Figures 7-10) indicates that as the air gap increases, the average room temperature is reduced due to the reduction in the area over that the heat transfer process takes place. It can be seen in figure 10 that by adding the fins to the surface of the absorber wall, its area increases and increases the absorption of sunlight, thus increasing the heat transfer compared to the absence of the fins. On the other hand, the presence of fins, especially rectangular fins, causes turbulence in the flow and increases the convection heat transfer coefficient, and thus increases the heat transfer.

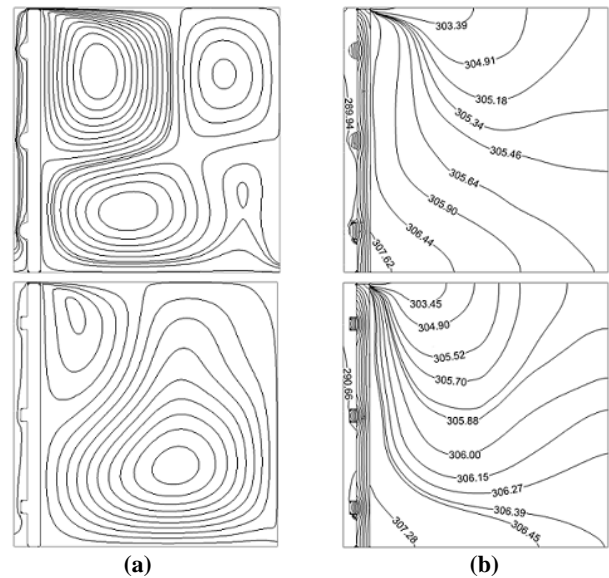
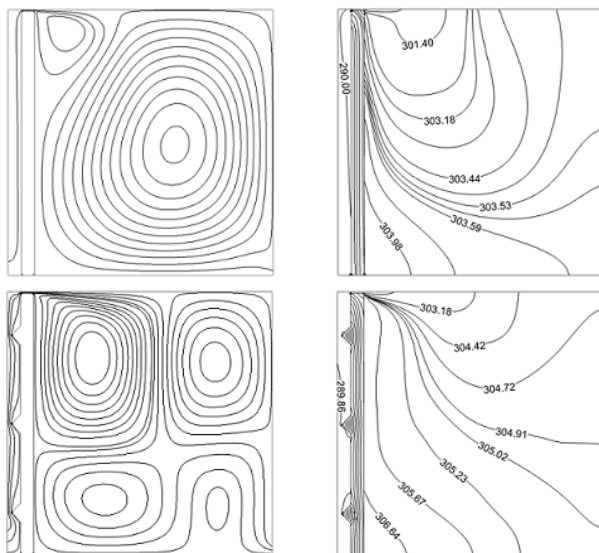


Figure 7. (a) Streamlines and (b) isotherms for  $Z_2 \approx 0.0m$

$$d_{sw} = 0.2 m, Z_1 = 0.5 m, Z_3 = 0.2 m \quad I = 500 \left( \frac{W}{m^2} \right)$$

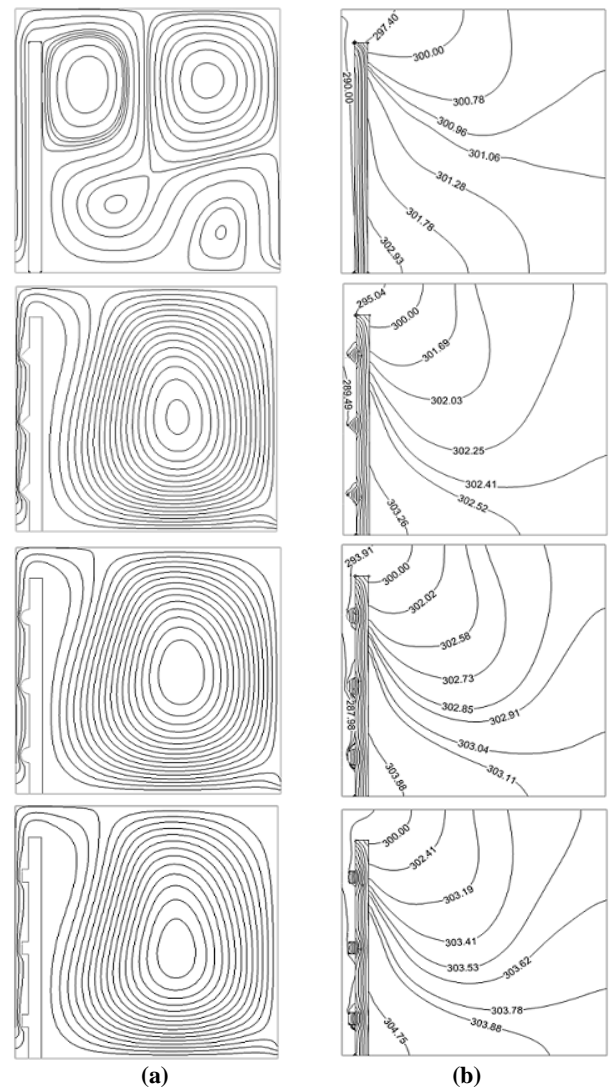


Figure 8. (a) Streamlines and (b) isotherms for  $Z_2 = 0.5m$ ,

$$d_{sw} = 0.2 m, Z_1 = 0.5 m, Z_3 = 0.2 m \quad I = 500 \left( \frac{W}{m^2} \right)$$

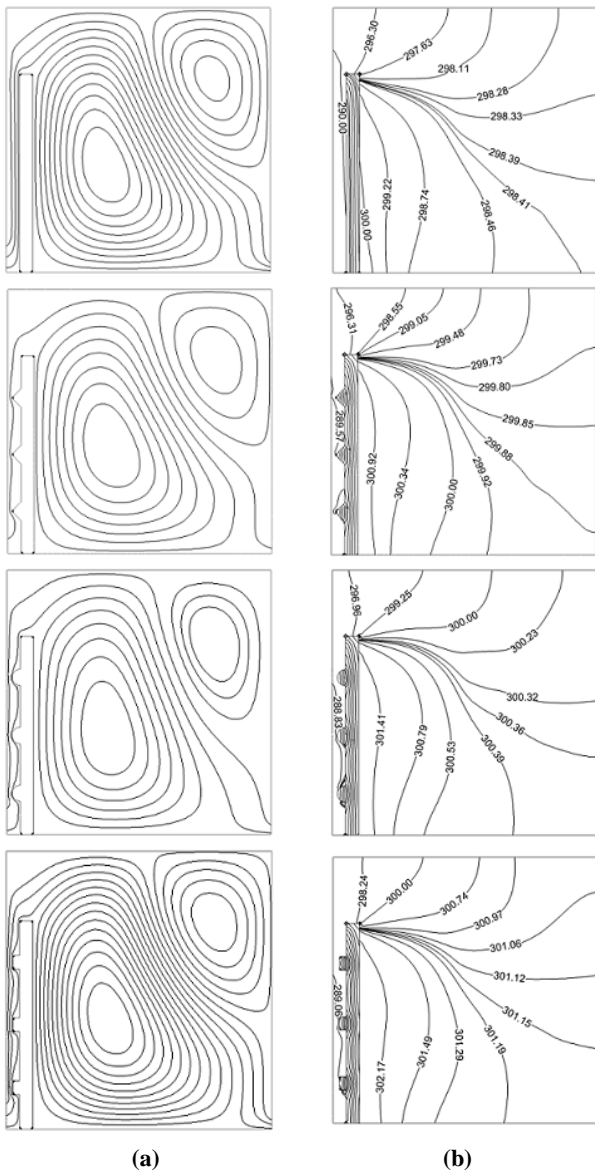


Figure 9. (a) Streamlines and (b) isotherms for  $Z_2 = 1.0m$ .

$$d_{sw} = 0.2 m, Z_1 = 0.5 m, Z_3 = 0.2m \quad I = 500 \left(\frac{W}{m^2}\right)$$

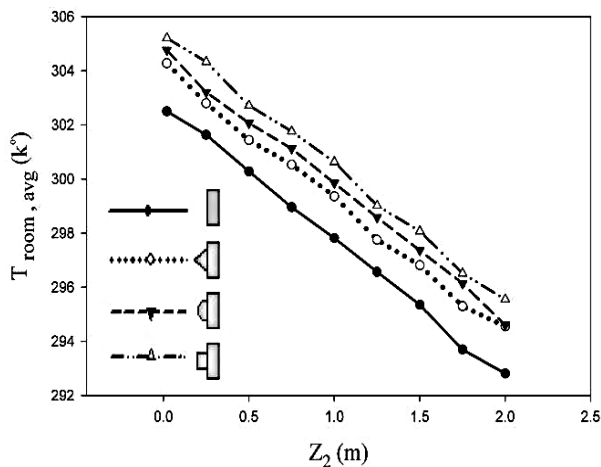


Figure 10. Comparison of average room temperature for different fin geometries at

$$d_{sw} = 0.2 m, Z_1 = 0.5 m, Z_3 = 0.2m \quad I = 500 \left(\frac{W}{m^2}\right)$$

### 6.2. Effect of radiation intensity

By increasing the radiation power, the energy absorbed by the Trombe wall is increased, which results in a larger temperature gradient, and this increases the buoyancy forces and the outlet flow. The air flow is heated near the solar wall and moves up to the ceiling due to its higher temperature. Then some of this heated air exits through the vents at the top of the solar wall and enters the room, which is at a lower temperature. Figure 11 shows the average room temperature at different radiation intensities for the base case without fins (11a) and with rectangular fins (11b). It should be noted that by increasing the size of the air gap, the changes in the average temperature versus distance are more significant.

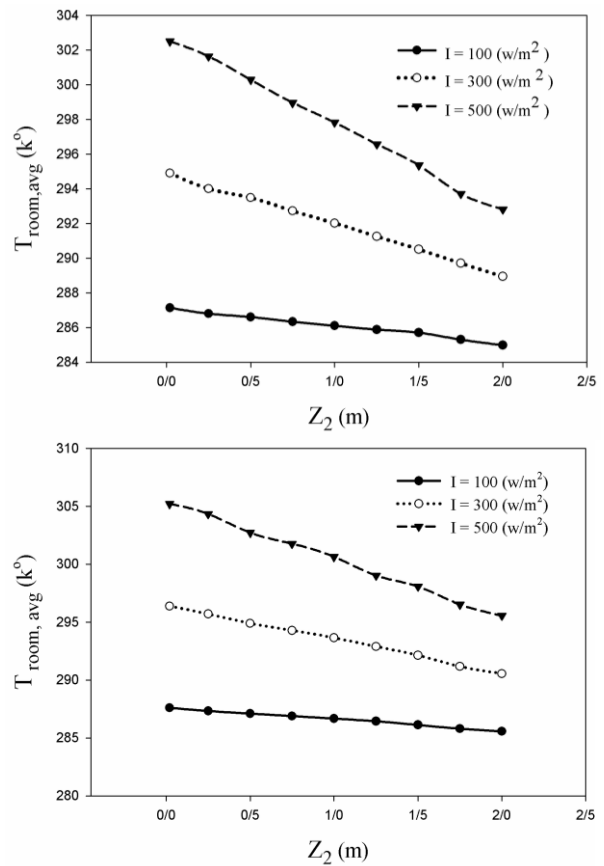


Figure 11. Room average temperature at different radiation intensities a) base case without fin, b) with rectangular fins at condition  $d_{sw} = 0.2 m, Z_1 = 0.5 m, Z_3 = 0.2 m, I = 500 \left(\frac{W}{m^2}\right)$ .

### 6.3. Effect of number of fins

Since the highest average room temperature was calculated for the rectangular fins, these fins were used for the other sensitivity analyses performed. The fins have the same shape and direction, and hence, by increasing the number of fins, the distance between them is reduced. Figure 12 shows the streamlines when the number of fins is increased. The results obtained show that the

number of vortices decreases, and instead, a large vortex of air circulation is formed in the system. Moreover, the isotherms shown in figure 13 indicate that increasing the number of fins leads to an increase in the temperature of the room. This is because the velocity of the air entering the vicinity of the fins has decreased, which results in a prolonged contact of air with the fins and increases the air temperature. However, there is an optimum value for the number of the fins since a higher number of fins causes overlapping of the boundary layer with the absorber's surface.

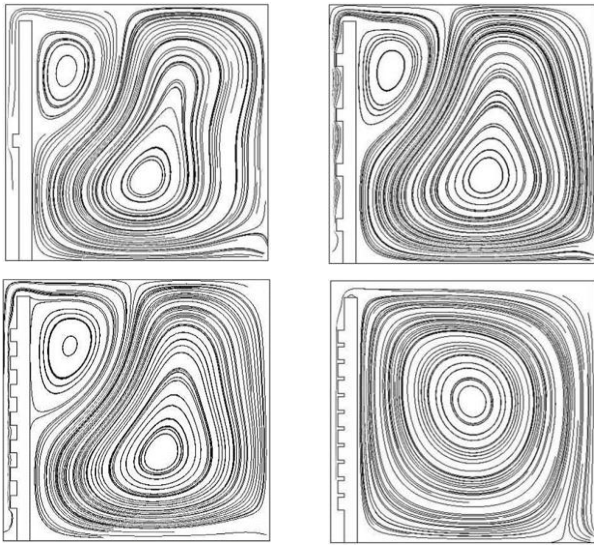


Figure 12. Streamlines at conditions  $d_{sw} = 0.2 \text{ m}$ ,  $Z_1 = 0.5 \text{ m}$ ,  $Z_2 = 0.25 \text{ m}$ ,  $Z_3 = 0.2 \text{ m}$ ,  $I = 500 \left(\frac{W}{m^2}\right)$ .

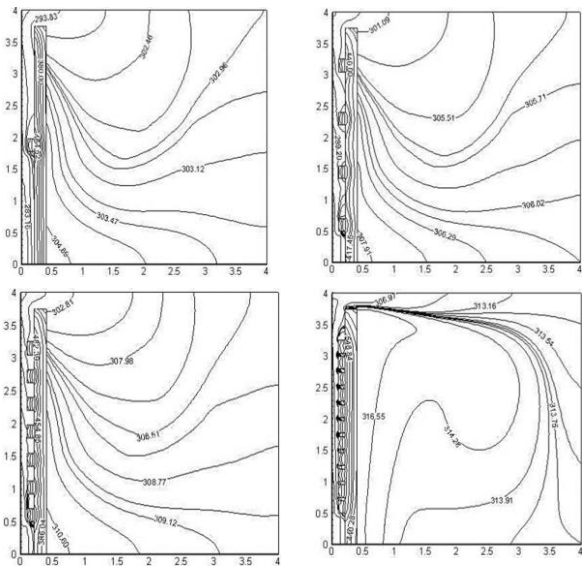


Figure 13. Isotherms calculated at  $d_{sw} = 0.2 \text{ m}$ ,  $Z_1 = 0.5 \text{ m}$ ,  $Z_2 = 0.25 \text{ m}$ ,  $Z_3 = 0.2 \text{ m}$ ,  $I = 500 \left(\frac{W}{m^2}\right)$ .

As mentioned above, increasing the number of fins (i.e. reducing the distance between the fins) increases the rate of heat transfer from the solar wall to the room. However, at a certain number of

fins, which was calculated to be eleven fins in this work, the rate of heat transfer decreased (Figure 14). This is because although the heat transfer area increases, the friction forces reduce the air velocity. This results in the stagnancy of the air between the fins and a reduction in the temperature gradient. Hence, it is vital to calculate the optimum number of fins to obtain the highest temperature in the room.

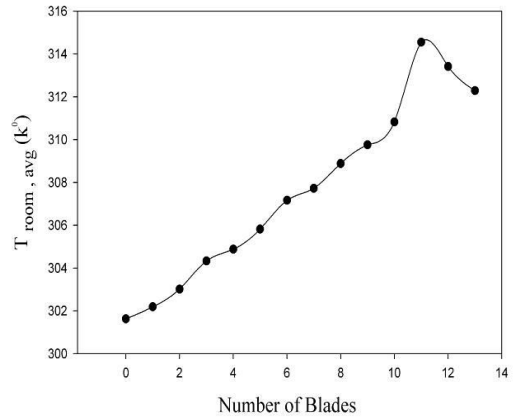


Figure 14. Room average temperature obtained by increasing number of fins at  $d_{sw} = 0.2 \text{ m}$ ,  $Z_1 = 0.5 \text{ m}$ ,  $Z_2 = 0.25 \text{ m}$ ,  $Z_3 = 0.2 \text{ m}$ ,  $I = 500 \left(\frac{W}{m^2}\right)$

#### 6.4. Effect of distance between absorber wall and glass surface

Figure 15 compares the calculated average room temperature at different distances between the absorber wall and the glass surface. Increasing the distance reduces the average room temperature. In this work, the optimal distance was calculated to be 0.2 m, at which the average room temperature was maximized.

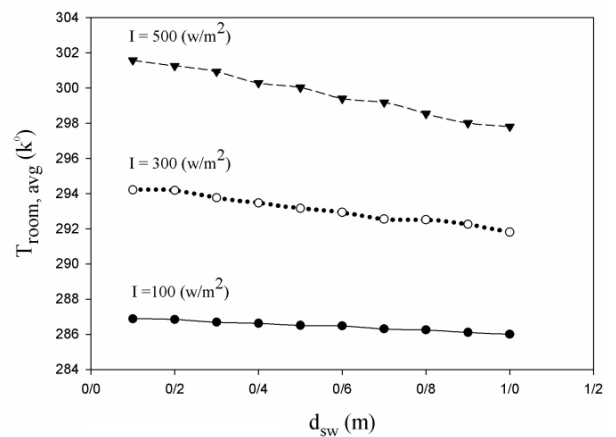


Figure 15. Comparison of average room temperature at different distances between absorber wall and glass surface.

#### 6.5. Effect of location of outlet vents

Figure 16 shows the average room temperature when the location of the outlet vents is changed.

The results obtained indicate that the vents' location does not affect the average room temperature. Hence, their location can be changed according to the interior design and in the best harmony with the room's facilities.

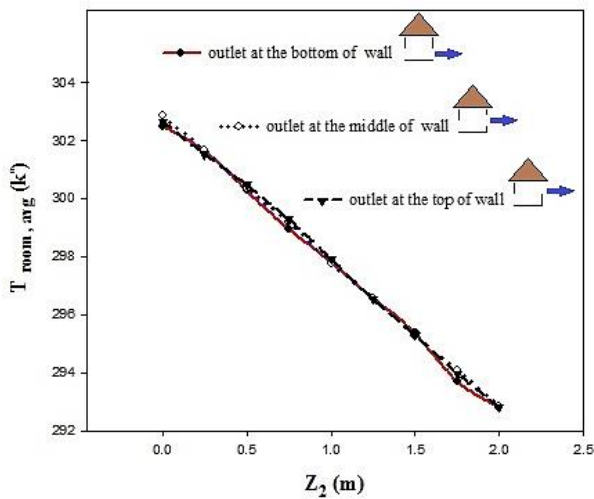


Figure 16. Effect of location of outlet vent on average room temperature.

## 7. Conclusions

In this work, a non-active heating system of a building using a solar wall was investigated. The objective of this work was to perform a sensitivity analysis on the parameters that affected the system. In order to achieve this aim, a solar wall system was simulated, and the results obtained were confirmed with the data reported in the literature. This case was used as a base case for the sensitivity analysis performed. The results of this work show that:

- Increasing the intensity of the radiation increases the energy absorbed by the Trombe wall, which results in a higher temperature gradient, buoyancy forces, and the air velocity at the outlet.
- Increasing the air gap reduces the average room temperature since the area of heat transfer decreases.
- The installation of fins on the absorber's surface increases the average room temperature. Among different fin geometries, the highest room temperature was calculated for the rectangular fin, which was 2.74 °C more than the other cases.
- The location of the outlet vents did not have an impact on the average room temperature, and could thus be changed according to the interior design of the room.
- The presence of the fins decreases the air circulation in the room, which provides more comfortable conditions for the dwellers.

f) Increasing the distance between the absorber wall and the glass surface reduces the average room temperature. This reduction is more severe in a high-intensity radiation.

g) Practically, the use of fins, especially rectangular fins, is recommended in a building design. Regarding the height of the absorber wall, if the discussion is about using the south light to illuminate the house, a shorter absorber wall is recommended; otherwise, a longer absorber wall is recommended for a real building. Also the location of the outlet valve has no effect on the amount of heat transfer, and can be arbitrarily selected to be in harmony with the architecture of the building.

## 8. References

- Zaniani, J. R., Ghahfarokhi, S. T., Jahangiri, M., and Shamsabadi, A. A. (2019). Design and optimization of heating, cooling, and lightening systems for a residential villa at Saman city, Iran. *Journal of Engineering, Design and Technology*. Vol. 17, No. 1, pp. 41-52.
- Mostafaeipour, A., Goudarzi, H., Sedaghat, A., Jahangiri, M., Hadian, H., Rezaei, M., and Karimi, P. (2019). Energy efficiency for cooling buildings in hot and dry regions using sol-air temperature and ground temperature effects. *Journal of Engineering, Design and Technology*. Vol. 17, No. 3, pp. 613-628.
- Kalbasi, R., Jahangiri, M., Nariman, A., and Yari, M. (2019). Optimal design and parametric assessment of grid-connected solar power plants in Iran, a review. *Journal of Solar Energy Research*, Vol. 4, No. 2, pp. 142-162.
- Kalbasi, R., Jahangiri, M., and Tahmasebi, A. (2021). Comprehensive Investigation of Solar-based Hydrogen and Electricity Production in Iran. *International Journal of Photoenergy*, Article ID 6627491.
- Kalbasi, R., Jahangiri, M., Mosavi, A., Dehshiri, S.J.H., Dehshiri, S.S.H., Ebrahimi, S., Etezadi, Z.A.S., and Karimipour, A. (2021). Finding the best station in Belgium to use residential-scale solar heating, one-year dynamic simulation with considering all system losses: economic analysis of using ETSW. *Sustainable Energy Technologies and Assessments*, Vol. 45, p. 101097.
- Yousefi, Y., Jahangiri, M., Shamsabadi, A. A., and Dehkordi, A. R. (2019). Designing a mediator space and the study of its effect on the energy consumption of a residential building using EnergyPlus software in Savadkuh, Iran. *Journal of Engineering, Design and Technology*. Vol. 17, No. 4, pp. 833-846.
- Pahlavan, S., Jahangiri, M., Alidadi Shamsabadi, A., and Khechekhouche, A. (2018). Feasibility study of solar water heaters in Algeria, a review. *Journal of Solar Energy Research*, Vol. 3, No. 2, pp. 135-146.

- [8] Jahangiri, M., Alidadi Shamsabadi, A., and Saghaei, H. (2018). Comprehensive evaluation of using solar water heater on a household scale in Canada. *Journal of Renewable Energy and Environment*, Vol. 5, No. 1, pp. 35-42.
- [9] Siampour, L., Vahdatpour, S., Jahangiri, M., Mostafaeipour, A., Goli, A., Shamsabadi, A.A., and Atabani, A. (2021). Techno-enviro assessment and ranking of Turkey for use of home-scale solar water heaters. *Sustainable Energy Technologies and Assessments*, Vol. 43, p. 100948.
- [10] Zaniani, J. R., Dehkordi, R. H., Bibak, A., Bayat, P., and Jahangiri, M. (2015). Examining the possibility of using solar energy to provide warm water using RETScreen4 software (case study: Nasr primary school of pirbalut). *Current World Environment*, Vol. 10, pp. 835- 841.
- [11] Nguyen, Q., Naghieh, A., Kalbasi, R., Akbari, M., Karimipour, A., and Tlili, I., 2021. Efficacy of incorporating PCMs into the commercial wall on the energy-saving annual thermal analysis. *Journal of Thermal Analysis and Calorimetry*, 143(3), pp. 2179-2187.
- [12] Nariman, A., Kalbasi, R., and Rostami, S. (2021). Sensitivity of AHU power consumption to PCM implementation in the wall-considering the solar radiation. *Journal of Thermal Analysis and Calorimetry*, Vol. 143, No. 3, pp. 2789-2800.
- [13] Motahar, S. and Jahangiri, M. (2020). Transient heat transfer analysis of a phase change material heat sink using experimental data and artificial neural network. *Applied Thermal Engineering*, Vol. 167, p. 114817.
- [14] Shamsabadi, A.A., Jahangiri, M., Rezaei, T., Farsani, R.Y., Seryani, A., and Hakim, S. (2021). The design of a seasonal heat storage system with a geothermal heat pump for a residential building in Tehran. *Journal of Engineering, Design and Technology*, in press.
- [15] Siampour, L., Vahdatpour, S., Jahangiri, M., Mostafaeipour, A., Goli, A., Shamsabadi, A. A., and Atabani, A. (2021). Techno-enviro assessment and ranking of Turkey for use of home-scale solar water heaters. *Sustainable Energy Technologies and Assessments*, Vol. 43, p. 100948.
- [16] Almutairi, K., Mostafaeipour, A., Baghaei, N., Techato, K., Chowdhury, S., Jahangiri, M., and Rezaei, M. (2021). Techno-Economic Investigation of Using Solar Energy for Heating Swimming Pools in Buildings and Producing Hydrogen: A Case Study. *Frontiers in Energy Research*, Vol. 9, p. 680103.
- [17] Du, L., Ping, L., and Yongming, C. (2020). Study and analysis of air flow characteristics in Trombe wall. *Renewable Energy*, Vol. 162, pp. 234-241.
- [18] Sergei, K., Shen, C., and Jiang, Y., (2020). A review of the current work potential of a trombe wall. *Renewable and Sustainable Energy Reviews*, Vol. 130, p. 109947.
- [19] Saadatian, O., Sopian, K., Lim, C.H., Asim, N., and Sulaiman, M.Y. (2012). Trombe walls: A review of opportunities and challenges in research and development. *Renewable and Sustainable Energy Reviews*, Vol. 16, No. 8, pp. 6340-6351.
- [20] Tan, A.Y.K. and Wong, N.H. (2013). Parameterization studies of solar chimneys in the tropics. *Energies*, Vol. 6, No. 1, pp. 145-163.
- [21] Salehpour, A., Sadatlu, M.A.A., and Sojoudi, A. (2019). Unsteady natural convection in a differentially heated rectangular enclosure possessing sinusoidal corrugated side walls loaded with power law non-Newtonian fluid. *Fluid Dynamics*, Vol. 54, No. 2, pp. 159-176.
- [22] Chan, H.Y., Riffat, S.B., and Zhu, J. (2010). Review of passive solar heating and cooling technologies. *Renewable and Sustainable Energy Reviews*, Vol. 14, No. 2, pp. 781-789.
- [23] Yedder, R.B., Du, Z.G., and Bilgen, E. (1990). Numerical study of laminar natural convection in composite trombe wall systems. *Solar and wind technology*, Vol. 7, No. 6, pp. 675-683.
- [24] Yedder, R.B. and Bilgen, E. (1991). Natural convection and conduction in Trombe wall systems. *International Journal of Heat and Mass Transfer*, Vol. 34, No. 4-5, pp. 1237-1248.
- [25] Gan, G. (2006). Simulation of buoyancy-induced flow in open cavities for natural ventilation. *Energy and buildings*, Vol. 38, No. 5, pp. 410-420.
- [26] Mezrhab, A. and Rabhi, M. (2008). Modeling of the thermal transfers in an enclosure of the Trombe wall type. *Thermodynamic analysis in renewable energy*, Vol. 10, No. 62, pp. 9-14.
- [27] Li, Y., Duanmu, X., Sun, Y., Li, J., and Jia, H. (2007). Study on the air movement character in solar wall system, In *Proceedings: Building Simulation*, pp. 927-931.
- [28] Kim, S. and Seo, J. (2012). An influence of the opening location of the trombe wall system on indoor airflow and thermal environment. *National Research Foundation of Korea*, pp. 1-6.
- [29] Mansour, A.R., Jubran, B.A., and Tashtoush, B., An approximate analytical solution to convective laminar heat transfer flow within the Trombe wall channel. *International communications in heat and mass transfer* (1991) Vol. 18, No. 1, pp. 153-159.
- [30] Jubran, B.A., Hamdan, M.A., Tashtoush, B., and Mansour, A.R., An approximate analytical solution for the prediction of transient response of the trombe wall. *International communications in heat and mass transfer* (1993), Vol. 20, No. 4, pp. 567-577.

- [31] Ong, K.S., A mathematical model of a solar chimney. *Renewable energy* (2003), Vol. 28, No. 7, pp. 1047-1060.
- [32] Haghghi, A.P. and Maerefat, M. (2014). Solar ventilation and heating of buildings in sunny winter days using solar chimney. *Sustainable Cities and Society*, Vol. 10, pp. 72-79.
- [33] Li, Z., Du, C., Ahmadi, D., Kalbasi, R., and Rostami, S. (2021). Numerical modeling of a hybrid PCM-based wall for energy usage reduction in the warmest and coldest months. *Journal of Thermal Analysis and Calorimetry*, Vol. 144, pp. 1985-1998.
- [34] Bergman T.L., Incropera F.P., DeWitt D.P., and Lavine A.S. (2011). *Fundamentals of heat and mass transfer*, New York: John Wiley and Sons.
- [35] Jahangiri, M., Saghafian, M., and Sadeghi, M. R. (2015). Effects of non-Newtonian behavior of blood on wall shear stress in an elastic vessel with simple and consecutive stenosis. *Biomedical and Pharmacology Journal*, Vol. 8, No. 1, pp. 123-131.
- [36] Jahangiri, M., Saghafian, M., and Sadeghi, M. R. (2015). Numerical simulation of hemodynamic parameters of turbulent and pulsatile blood flow in flexible artery with single and double stenoses. *Journal of Mechanical Science and Technology*, Vol. 29, No. 8, pp. 3549-3560.
- [37] Jahangiri, M., Haghani, A., Ghaderi, R., and Hosseini Harat, S. M. (2018). Effect of non-Newtonian models on blood flow in artery with different consecutive stenosis. *Journal of Advanced Design and Manufacturing Technology*, Vol. 11, No. 1, pp. 79-86.
- [38] Jahangiri, M., Saghafian, M., and Sadeghi, M. R. (2018). Effect of six non-Newtonian viscosity models on hemodynamic parameters of pulsatile blood flow in stenosed artery. *Journal of Computational and Applied Research in Mechanical Engineering*, Vol. 7, No. 2, pp. 199-207.
- [39] Yadegari, M. and Jahangiri, M. (2019). Simulation of non-Uniform Magnetic Field Impact on non-Newtonian and Pulsatile Blood Flow. *Journal of Advanced Research in Fluid Mechanics and Thermal Sciences*, Vol. 57, No. 1, pp. 86-99.
- [40] Khanal, R. and Lei, C. (2015). A numerical investigation of buoyancy induced turbulent air flow in an inclined passive wall solar chimney for natural ventilation. *Energy and Buildings*, Vol. 93, pp. 217-226.
- [41] Launder, B.E. and Spalding, D.B. (1983). *Numerical prediction of flow, heat transfer, turbulence and combustion*, pp. 96-116, Amsterdam: Elsevier Ltd.
- [42] Moradicheghamahi, J., Jahangiri, M., Mousaviraad, M., and Sadeghi, M. R. (2020). Computational studies of comparative and cumulative effects of turbulence, fluid-structure interactions, and uniform magnetic fields on pulsatile non-Newtonian flow in a patient-specific carotid artery. *Journal of the Brazilian Society of Mechanical Sciences and Engineering*, Vol. 42, No. 10, pp. 1-22.
- [43] Sharifzadeh, B., Kalbasi, R., and Jahangiri, M. (2020). The effect of turbulence model on predicting the development and progression of coronary artery atherosclerosis. *Journal of Computational and Applied Research in Mechanical Engineering*, Vol. 10, No. 1, pp. 183-199.
- [44] Jahangiri, M., Saghafian, M., and Sadeghi, M. R. (2014). Numerical study of hemodynamic parameters in pulsatile turbulent blood flow in flexible artery with stenosis. In the 22nd annual international conference on mechanical engineering-ISME2014, Shahid Chamran University, Ahvaz, Iran, pp. 1-5.
- [45] Jafari, A. and Poshtiri, A.H. (2017). Passive solar cooling of single-storey buildings by an adsorption chiller system combined with a solar chimney. *Journal of cleaner production*, Vol. 141, pp. 662-682.
- [46] Duffie, J.A. and Beckman, W.A. (1980). *Solar engineering of thermal processes*. New York: John Wiley and Sons.